

Modeling Green's function measurements with two-tip scanning tunneling microscopy

Leeuwenhoek, Maarten; Gröblacher, Simon; Allan, Milan P.; Blanter, Yaroslav M.

DOI

[10.1103/PhysRevB.102.115416](https://doi.org/10.1103/PhysRevB.102.115416)

Publication date

2020

Document Version

Final published version

Published in

Physical Review B

Citation (APA)

Leeuwenhoek, M., Gröblacher, S., Allan, M. P., & Blanter, Y. M. (2020). Modeling Green's function measurements with two-tip scanning tunneling microscopy. *Physical Review B*, *102*(11), Article 115416. <https://doi.org/10.1103/PhysRevB.102.115416>

Important note

To cite this publication, please use the final published version (if applicable). Please check the document version above.

Copyright

Other than for strictly personal use, it is not permitted to download, forward or distribute the text or part of it, without the consent of the author(s) and/or copyright holder(s), unless the work is under an open content license such as Creative Commons.

Takedown policy

Please contact us and provide details if you believe this document breaches copyrights. We will remove access to the work immediately and investigate your claim.

Modeling Green's function measurements with two-tip scanning tunneling microscopy

Maarten Leeuwenhoek,^{1,2} Simon Gröblacher^{1,*}, Milan P. Allan^{2,†} and Yaroslav M. Blanter^{1,‡}
¹*Department of Quantum Nanoscience, Kavli Institute of Nanoscience, Delft University of Technology, Lorentzweg 1, 2628CJ Delft, Netherlands*

²*Leiden Institute of Physics, Leiden University, Niels Bohrweg 2, 2333CA Leiden, Netherlands*



(Received 8 May 2020; accepted 28 August 2020; published 14 September 2020)

A double-tip scanning tunneling microscope with nanometer-scale tip separation has the ability to access the single-electron Green's function in real and momentum spaces based on second-order tunneling processes. Experimental realization of such measurements has been limited to quasi-one-dimensional systems due to the extremely small signal size. Here we propose an alternative approach to obtain such information by exploiting the current-current correlations from the individual tips and present a theoretical formalism to describe it. To assess the feasibility of our approach we make a numerical estimate for an ~ 25 -nm Pb nanoisland and show that the wave function in fact extends from tip to tip and the signal depends less strongly on increased tip separation in the diffusive regime than the one in alternative approaches relying on tip-to-tip conductance.

DOI: [10.1103/PhysRevB.102.115416](https://doi.org/10.1103/PhysRevB.102.115416)

I. INTRODUCTION

Green's functions provide a general framework for perturbed and interacting electron systems. Direct experimental access to the electron Green's function is vital for our understanding of (new) complex systems and electronic states of matter. This access is increasingly provided by the emergence of spectroscopic imaging scanning tunneling microscopy (SI-STM) and by various types of angle-resolved photoemission spectroscopy experiments. A further possible tool for probing the single-electron Green's function locally is double-tip STM, where two tips are brought into tunneling simultaneously within a few (tens of) nanometers apart [1–3]. The challenge of accessing the Green's function using a two-probe setup is twofold: (i) Since it is a second-order tunneling process, the signal depends strongly on both the tip-to-sample and tip-to-tip distances [1,2,4], and (ii) experimental realization of such a small tip separation in combination with the stringent stability requirements STM brings has proven challenging and has been a long-standing goal for the multiprobe community [5].

Here we explore and present a theoretical formalism for an alternative approach which, using a double-tip STM, has access to the propagator—an averaged product of two single-electron Green's functions. The propagator determines the nature of electron wave propagation and is essential for understanding quantum effects in electron transport. Here we show that it can be measured locally, between the points corresponding to the tip positions. The advantage of this approach is that, compared with the approach mentioned above, the result is not exponential in terms of tip-to-tip distance, at the cost of having a higher power of the tip-sample tunneling

amplitude. We concentrate on the diffusive regime of electron transport and show that by calculating statistical correlations between the individual currents from the tips to the sample we can access the diffusion propagator at the nanoscale. Using the proposed formalism, we performed initial numerical estimates on Pb nanoislands to demonstrate the feasibility of this approach.

Much progress has been made over the past few decades towards a stable, well-controlled double-tip microscope [6] able to probe the local Green's function by reducing tip radii and increasing their aspect ratio [7–10], low-temperature and/or ultrahigh-vacuum (UHV) operation [11–13], mechanical stability [14,15], and navigation of the tips [7,16]. Recently, we have seen a reemergence of the double-tip STM [7,17], culminating in the first two-point single-electron Green's function measurements to date using a multiprobe system on quasi-one-dimensional dimer rows on the Ge(001) surface [18].

In parallel we observed a similar resurgence of nanofabricated STM probes [19–21] that can be equipped with two (fixed) probes that are compatible with ultrahigh vacuum and low-temperature operation and potentially allow the integration in ultrastable single-tip STM systems currently available [21]. Advances in modern nanofabrication techniques such as focused ion beam milling and electron beam induced deposition could lead to a tip separation of a few tens of nanometers in the very near future. Driven by this experimental progress, we outline the theory for our measurement formalism here and make a numerical estimate to assess its feasibility.

In Sec. II we recap earlier proposals for measuring the electron Green's function with a double-tip STM. Subsequently, in Sec. III we discuss the current correlations and show that they are proportional to the diffusion propagator. In the same section, we produce numerical estimates of the effect and show that it can be measured using the current technology. We present conclusions in Sec. IV. Some technical details from the derivation of Sec. III are relegated to the Appendix.

*s.groblacher@tudelft.nl

†allan@physics.leidenuniv.nl

‡y.m.blanter@tudelft.nl

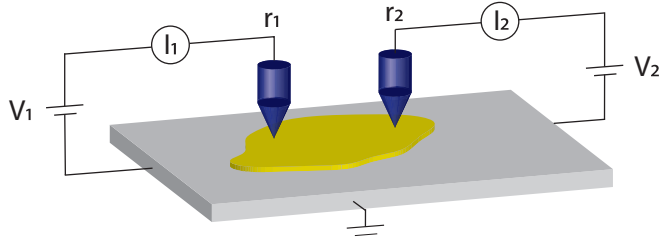


FIG. 1. Schematic of a two-tip setup on a mesoscopic island.

II. MEASURING GREEN'S FUNCTIONS WITH STM INVOLVING TWO TIPS

Before we outline our alternative tools that use current-current correlations to probe the electronic states we first briefly introduce the method proposed by Refs. [1,2] that shares the same three-terminal setup. The tips and the sample are kept at constant chemical potentials: tip 1 (μ_1), tip 2 (μ_2), and the sample (μ_0), and similar to single-probe STM, both tips are individually biased (V_1, V_2), and their respective currents are measured (I_1, I_2) as shown in Fig. 1. The response of currents to voltages is described by the conductance matrix σ_{ij} , $I_i = \sigma_{ij}V_j$.

In a usual STM experiment only the response of the current in a tip to the voltage applied between the tip and the sample is measured. For the two-probe setup this translates into diagonal elements of the conductance matrix, σ_{11} and σ_{22} , which are proportional to the local density of states at the locations of the tips. With the two-probe setup one can also obtain the off-diagonal elements σ_{12} and σ_{21} that contain information about transport properties of the electrons inserted at one tip and collected on the other. In fact, this complementary information should allow us, in principle, to obtain the full single-electron Green's function [1].

The transport is described by a cotunneling process with the sample as the intermediate state. The properties of this process can be derived using Fermi's golden rule to second order and result in a transconductance $\sigma_{21} = \partial I_2 / \partial V_1$ [22]. The same expression, albeit in a slightly different form, was obtained in the original work [1,2] when looking at second-order transport,

$$\sigma_{21} = \frac{\partial I_2}{\partial V_1} = \Gamma_1 \Gamma_2 \frac{2\pi e^2}{\hbar} |G(\mathbf{r}_1, \mathbf{r}_2; \epsilon = \mu_1)|^2, \quad (1)$$

where $G(\mathbf{r}_1, \mathbf{r}_2; \epsilon)$ is the retarded Green's functions of the sample for noninteracting electrons at zero temperature and Γ_1, Γ_2 are the tunnel rates from the tips to the substrate, which in Ref. [2] were related to the matrix elements of the tunnel Hamiltonian. We note that the signal size is now quadratic in tip-sample coupling and $|G(\mathbf{r}_1, \mathbf{r}_2)|$ is on the order of 10^{-2} for two-dimensional (2D) systems and a tip-to-tip distance of a few tens of nanometers and is inversely proportional to that distance [1]. A similar result can be obtained using the Landauer formalism following Settnes *et al.* [3,4]. Unsurprisingly, the first double-tip STM results were taken on a quasi-one-dimensional system [18] where the signal is stronger overall and does not decay with tip separation.

Technical considerations

The technical development of the double-tip STMs has been led by the multiprobe community that originally focused on studying resistance in mesoscopic systems on (sub)micrometer length scales by contacting the surface with, ideally, four probes. An intrinsically simpler double-tip STM designed for Green's function mapping uses only two tips to probe the single-electron Green's function; however, it requires operation in the tunneling (not contact) regime, prolonged out-of-feedback measurements, and nanometer tip separation. Therefore, mechanical stability and tip-to-tip distance make up the main challenges that need to be addressed.

For the latter, the radii of curvature of the tips need to be reduced to the (tens of) nanometer range to achieve tip separation that is effectively set by twice the tip radius. Tips made by well-controlled tungsten etching, sharpened by focused ion beam milling or equipped with metallized carbon nanotubes, are used to create extremely sharp, high aspect ratio tips capable of achieving tip separations down to 30 nm [7]. Being able to navigate the two tips to such proximity that the scanning range of each tip overlaps has proven challenging as well, especially without any optical input. Several solutions have been explored [16,23], resulting in an additional scanning electron microscope (SEM) column as the most common solution [24–26]. The separate piezo drives for each tip together with the SEM column make for a more complex and elaborate apparatus, making it more challenging to achieve very low temperatures and rival the stability of compact single-tip STM designs [6,15], but recently that has been changing [25] and has paved the road to the first transconductance measurements to date [18].

Some of the navigation and stability issues can also be overcome by relocating the complexity of two probes from the STM head design to the tip itself, i.e., by having two nanofabricated tips fixed on a single device [21,27–29]. Such devices can, indeed, be implemented in (commercially available) ultrastable single-tip STM systems that operate at low-temperature and UHV conditions [21]. Future application for controlled double-tip experiments will depend on the ability to get both tips into tunneling simultaneously with good stability.

III. PROPAGATOR FROM THE CURRENT CORRELATIONS: THEORETICAL CONSIDERATION FOR MEASURING THE DIFFUSION PROPAGATOR

To further assist the recent experimental progress we outline the theory for an alternative experiment using two tips on a nanoisland to probe the propagator $\Pi(\mathbf{r}_1, \mathbf{r}_2)$ at the nanoscale and highlight the feasibility of our approach with numerical estimates. Whereas we focus on and make estimates for the regime of diffusive motion of electrons, the principle is more general and applies to any underlying electron dynamics. We note that this is just one example of accessing Green's functions with double tips; others are mentioned above [1–4,30–32]. Our example has the advantage of being simpler and yielding an improvement of the signal strength. It is based on correlating the two measured single-tip currents in order to obtain correlations between electron states

at the respective tip positions and to ultimately measure the electronic diffusion propagator on the nanoscale.

In this section, we first describe the specific setup we are considering here. We then derive an explicit expression of the diffusion propagator as a function of our experimental observables. By exploiting the formalism of level and wave function statistics developed earlier [33,34], we show that the correlations of the amplitude of the same wave function are sustained even at these relatively large distances (much larger than the Fermi wavelength), while the correlations between different wave functions decay, resulting in the expression that relates the measured currents to the diffusion propagator. Finally, we apply the formalism to metallic nanoislands and provide some numerical estimates that yield the required sizes of the double tips.

A. Preliminaries

The scenario considered here consists of two tips held at individual bias voltages V_i while measuring the individual currents I_i . The sample is grounded, which considerably simplifies the experiment. We assume a smart tip consisting of two tips located at \mathbf{r}_1 and \mathbf{r}_2 , with the distance between the tips being much longer than the Fermi wavelength. As a starting point for the theoretical description of the tunneling process we consider the Tersoff-Hamann model of STM [35], with the tunneling current from each tip to the substrate being [36]

$$I(\mathbf{r}, V) = B \int_0^{eV} n^s(\mathbf{r}, E) dE. \quad (2)$$

Here E is the energy, and B is the tip-sample coupling, which includes details of the tunneling process of the tip and is exponentially dependent on the tip-to-sample distance. The order of magnitude of B is G_T/ν , with G_T and ν being the tunneling conductance (tip to substrate) and the density of states (per volume) in the substrate. The information about the substrate is encoded in the function n^s ,

$$n^s(\mathbf{r}, E) = \sum_k \delta(E - E_k) |\psi_k(\mathbf{r})|^2, \quad (3)$$

where E_k and ψ_k are the exact eigenvalues and eigenfunctions of an electron in the substrate.

In the following, we focus on weakly disordered metals, where $k_F l \gg 1$, with k_F and l being the Fermi wave vector and the mean free path, respectively. In this situation, the exact energies and wave functions in Eq. (3) depend on the disorder configuration, and one needs to look at the average values.

Before treating the double-tip situation, we calculate the disorder-averaged tunneling current for a single tip. The average square modulus of the wave function is a constant and, due to the normalization condition, equal to the inverse area \mathcal{A} of the substrate (assuming the geometry is 2D). Then

$$\langle n^s(\mathbf{r}, E) \rangle = \frac{1}{\mathcal{A}} \left\langle \sum_k \delta(E - E_k) \right\rangle = \nu.$$

Note that the result does not depend on the position or on the energy. This is the result of standard approximations we implicitly made. The energy independence is guaranteed by the fact that we are working close to the Fermi energy, where the density of states is constant. The density of states can be position dependent in a situation when electrons experience some external position-dependent force, for example, in an inhomogeneous sample. Whereas our method works for this case as well, all estimates below are made for the homogeneous case.

For the average current we thus have $\langle I(\mathbf{r}, V) \rangle = B\nu eV$. It is position independent and proportional to the voltage.

B. Correlations of the tunneling current

Next, we derive an expression for the current correlations in a double-tip configuration. Our aim is to bring the expression to a form that relates it directly to the observables of the experiment, which are the individual currents and their cumulant,

$$\begin{aligned} J(\mathbf{r}_1, \mathbf{r}_2; V_1, V_2) &= \langle \langle I(\mathbf{r}_1, V_1) I(\mathbf{r}_2, V_2) \rangle \rangle \\ &= B_1 B_2 \int_0^{eV_1} dE_1 \int_0^{eV_2} dE_2 \langle \langle n^s(\mathbf{r}_1, E_1) n^s \\ &\quad \times (\mathbf{r}_2, E_2) \rangle \rangle. \end{aligned} \quad (4)$$

The double brackets $\langle \langle \cdot \rangle \rangle$ are defined by $\langle \langle UW \rangle \rangle \equiv \langle UW \rangle - \langle U \rangle \langle W \rangle$. We have introduced two different constants, B_1 and B_2 , for different tips. In this expression, the key term to calculate is

$$\begin{aligned} \langle \langle n^s(\mathbf{r}_1, E_1) n^s(\mathbf{r}_2, E_2) \rangle \rangle &= -\nu^2 + \delta(E_1 - E_2) \left\langle \sum_k \delta(E_k - E_1) |\psi_k(\mathbf{r}_1) \psi_k(\mathbf{r}_2)|^2 \right\rangle \\ &\quad + R(E_1 - E_2) \times \left\langle \sum_{k \neq l} \delta(E_1 - E_k) \delta(E_2 - E_l) |\psi_k(\mathbf{r}_1) \psi_l(\mathbf{r}_2)|^2 \right\rangle, \end{aligned} \quad (5)$$

where $R(\omega)$ is the level-level correlation function. The first term in Eq. (5) is just a product of the averages; it creates a contribution to J which is proportional to $V_1 V_2$ and is otherwise position independent and can therefore be ignored. It is the second term that is of interest here, and we will refer to it as the same-level correlation term. It describes the correlations of the same state at different points in space, and we will

estimate it in the following paragraphs. The last term describes the correlations of different states and hence contains the level-level correlation function. We show in the Appendix that in diffusive systems it can also be neglected.

The averages that form the same-level correlation term were calculated previously in the context of level and wave function statistics [33,34], and we want to sketch only the

main steps here. For low energies $|E_1 - E_2| \ll E_c$, with $E_c \equiv 2\pi \hbar D/L^2$ being the Thouless energy, we obtain

$$\left\langle \sum_k \delta(E_k - E_1) |\psi_k(\mathbf{r}_1) \psi_k(\mathbf{r}_2)|^2 \right\rangle = \Delta v^2 \begin{cases} k_d(r)[1 + \Pi(\mathbf{r}_1, \mathbf{r}_2)] + \Pi(\mathbf{r}_1, \mathbf{r}_2), & \eta = 1, \\ [1 + 2k_d(r)][1 + \Pi(\mathbf{r}_1, \mathbf{r}_2)], & \eta = 2, \end{cases} \quad (6)$$

and

$$\left\langle \sum_{k \neq l} \delta(E_k - E_1) \delta(E_l - E_2) |\psi_k(\mathbf{r}_1) \psi_l(\mathbf{r}_2)|^2 \right\rangle = v^2 k_d(r) \eta \Pi(\mathbf{r}_1, \mathbf{r}_1). \quad (7)$$

Here $r = |\mathbf{r}_1 - \mathbf{r}_2|$, $D = v_F^2 \tau / 2$ is the diffusion constant, v_F is the Fermi velocity, $\tau = l/v_F$ is the scattering time of the electrons, $L \sim \sqrt{A}$ is the typical linear size of the substrate, and $\Delta = (vA)^{-1}$ is the mean level spacing for electrons in the substrate. In the metallic diffusive regime, we have $L \gg l$. The short-range function $k_d(r) = \exp(-r/l) J_0^2(k_F r)$ decays at the scale of the Fermi wavelength and, since the tips cannot be arranged so closely, does not play a significant role in the correlations. The propagator Π can be expressed in terms of the single-electron Green's function as

$$\Pi(\mathbf{r}_1, \mathbf{r}_2) = 2\pi v \langle G^R(\mathbf{r}_1, \mathbf{r}_2, \varepsilon) G^A(\mathbf{r}_2, \mathbf{r}_1, \varepsilon) \rangle, \quad (8)$$

where G^R and G^A denote retarded and advanced electron Green's functions, respectively. Note that the expression does not depend on the energy ε as soon as it is taken close to the Fermi surface. We focus here on the metallic diffusive regime, when the diffusion propagator Π is the solution of the diffusion equation [33,34],

$$-D \nabla_1^2 \Pi(\mathbf{r}_1, \mathbf{r}_2) = \frac{1}{\pi v} \left[\delta(\mathbf{r}_1 - \mathbf{r}_2) - \frac{1}{A} \right],$$

where ∇_1 acts on \mathbf{r}_1 . The equation is supplemented by the boundary condition $\mathbf{n} \nabla_1 \Pi(\mathbf{r}_1, \mathbf{r}_2) = 0$, with \mathbf{n} being the normal to the boundary. However, it is also important that Eqs. (6)–(8) are general and can be applied to any underlying dynamic of electron motion, not just to the diffusive regime. For example, in Ref. [37] they were used to describe the correlation of wave functions in a ballistic system with a disordered boundary. One can think of further applications, such as hybrid systems, including normal metals and superconductors.

Finally, the parameter η in Eq. (7) is responsible for the magnetic field dependence. We discriminate between the two situations, the case when the external magnetic field is present to break the time-reversal symmetry ($\eta = 1$) and the case where it is absent (orthogonal symmetry, $\eta = 2$). Whereas the results for both symmetries do not have an explicit dependence on the magnetic field, there is a crossover between them which occurs roughly when the magnetic flux through the system is equal to the flux quantum.

We disregard the terms with k_d , and Eq. (6) becomes

$$\left\langle \sum_k \delta(E_k - E_1) |\psi_k(\mathbf{r}_1) \psi_k(\mathbf{r}_2)|^2 \right\rangle = \eta \Delta v^2 \Pi(\mathbf{r}_1, \mathbf{r}_2). \quad (9)$$

We will see below that the correlation function of the currents is proportional to the voltage, allowing us to directly obtain the diffusion propagator.

We now calculate the contribution of the term with $\delta(E_1 - E_2)$ in Eq. (5). The frequency integral is easily evaluated to give

$$J_1(\mathbf{r}_1, \mathbf{r}_2; V_1, V_2) = B_1 B_2 v^2 [\eta \Delta \min(eV_1, eV_2) \Pi(\mathbf{r}_1, \mathbf{r}_2) - e^2 V_1 V_2]. \quad (10)$$

The second term is the product of average currents, and thus, the first one (which is much smaller) contains information about the electron states. Note that this term trivially depends on the voltage and on the magnetic field. The presence of the correlations proves that the states spatially extend from \mathbf{r}_1 to \mathbf{r}_2 . The dependence on the tip-to-tip distance given by the diffusion propagator can be probed by repeating the experiment with different double-tip separations.

As we are interested in the autocorrelations of the shared energy levels between the two tips obtained from the current on each of the individual tips, it is not necessary to measure small currents like the transconductance suggested by Niu *et al.* [1] and Byers and Flatté [2]. We normalize the correlation function with the individual currents $\langle I_i \rangle = B_i v e V_i$ for $i = 1, 2$, and setting $V_1 = V_2 = V$, Eq. (10) then reduces to our final result:

$$\frac{J(\mathbf{r}_1, \mathbf{r}_2, V, V)}{\langle I_1 \rangle \langle I_2 \rangle} = \frac{\eta \Delta}{eV} \Pi(\mathbf{r}_1, \mathbf{r}_2) - 1. \quad (11)$$

This equation directly relates the diffusion propagator to the current correlation normalized by the individual currents. We also note that while the correlations can be long range, one needs nanometer range separation of the tips to measure the diffusion propagator (see numerical estimates below).

To reiterate, Eq. (11) is valid in the metallic diffusive regime, $k_F^{-1} \ll l \ll L$, and under the condition that the voltage is lower than the Thouless energy, $eV \ll E_c$. These conditions also imply that the dimensionless conductance $g = E_c/\Delta$ is much greater than 1.

Whereas the above calculation is for zero temperature, one can estimate the effect of temperature from Eq. (11). The role of the temperature is to involve more electron levels in the current by increasing their occupation. It is similar to the role of the voltage, which increases the number of levels involved by increasing the energy tunneling window. Therefore, the temperature dependence of Eq. (11) is qualitatively the same as the voltage dependence. In particular, for $eV \ll k_B T \ll E_c$ we expect that the first term in Eq. (11) is proportional to T^{-1} .

C. Numerical estimates and feasibility

Finally, we present some numerical estimates to show the feasibility of our approach. We consider a Pb nanoisland on which we scan with the two probes. We set the tip separation distance to $r = 20$ nm, a spacing that we consider experimentally viable in the near future and that fits well within a 25-nm island. The small volume of islands gives rise to the substantial level spacing that we require. Since we prefer an atomically flat surface that fits both tips, we consider a flat island of near-monolayer thickness previously obtained [38] and studied by STM [39–41]. Here we use an already

realizable 25-nm island that is three monolayers thick that has a level spacing of 0.68 meV (for a circular geometry) [40,41]. Our aim is to find an estimate for the signal in Eq. (11) in such a scenario.

We start by estimating the diffusion coefficient, $D = v_F^2 \tau / 2$. From the residual resistivity ratio in the thin-film lead we can determine its low-temperature resistivity [42], and using Ohm's law, we find the scattering time for Pb $\tau = m / (ne^2 \rho_{4K}) = 5.3 \times 10^{-13}$ s. Here e is the electron charge, and we used the low-temperature resistivity $\rho_{4K} = 9.7 \times 10^{-2} \mu\Omega$ cm, the effective electron mass $m = 1.9m_e$ [43], and the total density of valence electrons $n = 13.2 \times 10^{22} \text{ cm}^{-3}$. Taken together, these values give us a diffusion coefficient of $D = 223 \text{ cm}^2/\text{s}$.

The size of the island and the diffusion constant, as calculated above, result in a Thouless energy $E_c = (2\pi \hbar D) / \pi L^2 = 47 \text{ meV}$ (we have assumed a circular shape of the substrate), and together with the mean level spacing, the dimensionless conductance $g = E_c / \Delta = 206$. This value satisfies the condition $g \gg 1$ to make the approximation (see Eq. (3.56) in Ref. [34]) $\Pi(\mathbf{r}_1, \mathbf{r}_2) \approx (\pi g)^{-1} \ln(L/r) = 3.5 \times 10^{-4}$. Including the prefactors, in the absence of a magnetic field and with a bias voltage of 1.5 meV, we expect the measured ratio in Eq. (11) to be of the order of 10^{-4} , which can be increased by almost an order of magnitude by moving to monolayer films. We have thus shown that it is, in principle, possible to measure the diffusion propagator using realistic double-tip parameters. We would also like to note that this is only one example of an experiment using the developed smart- and double-tip platforms among many others [1–4,30–32].

IV. CONCLUSIONS

Motivated by the experimental progress on the realization of double-tip STMs, we presented an alternative formalism for probing such electron correlations on the atomic scale. By calculating the current-current correlations between the two tips for disordered metals we have shown that the spatial overlap of the wave functions can, in fact, reach from one tip to the other. In the diffusive limit we also notice that the decay of the signal is logarithmic with increasing tip separation and therefore slower in the ballistic limit [1]. To explore the feasibility of the proposed experiment we performed numerical estimates, and we showed that there is a significant signal to detect. We believe this alternative approach for acquiring electron correlation at the nanoscale may prove interesting as the experiment becomes possible and could contribute to reigniting interest in the largely unexplored possibilities of double-tip STM.

ACKNOWLEDGMENTS

This project was financially supported by the European Research Council (ERC StG Strong-Q and SpinMelt) and by the Netherlands Organisation for Scientific Research (NWO/OCW), as part of the Frontiers of Nanoscience program, as well as through Vidi grants (Grants No. 680-47-536 and No. 680-47-541).

APPENDIX: LEVEL-LEVEL CORRELATIONS

This Appendix is to evaluate the contribution of the last term in Eq. (5). We will show that its contribution to J is less important than the first term in Eq. (10) but that it has nontrivial voltage dependence. Since for a single experiment the distance between the two tips is fixed, we can use this nontrivial voltage dependence to look at correlations between different states in the system.

The level-level correlation function $R(\omega)$ is, in the lowest order, given by the Wigner-Dyson statistics. The theory of random matrices, from which the Wigner-Dyson statistics originates, discriminates between two situations: the absence of external magnetic field (Gaussian orthogonal ensemble, or GOE, $\eta = 2$) and the presence of magnetic field (Gaussian unitary ensemble, or GUE, $\eta = 1$). In GUE we have

$$R(\omega) = 1 - \left(\frac{\pi\omega}{\Delta} \right)^{-2} \sin^2 \left(\frac{\pi\omega}{\Delta} \right). \quad (\text{A1})$$

We disregarded the contribution of Eq. (7) in the main text due to the strong decay of k_d with distance. However, there is a long-range contribution to Eq. (7) which we have not taken into account because it has a higher order in g^{-1} terms in Eq. (7). Namely, we have [33,34]

$$\left\langle \sum_{k \neq l} \delta(E_k - E_1) \delta(E_l - E_2) |\psi_k(\mathbf{r}_1) \psi_l(\mathbf{r}_2)|^2 \right\rangle \rightarrow \frac{\eta}{2} v^2 \Pi^2(\mathbf{r}_1, \mathbf{r}_2). \quad (\text{A2})$$

Furthermore, for energies ω exceeding the Thouless energy E_c , $|E_1 - E_2| \gg E_c \gg \Delta$, we have

$$\left\langle \sum_{k \neq l} \delta(E_k - E_1) \delta(E_l - E_2) |\psi_k(\mathbf{r}_1) \psi_l(\mathbf{r}_2)|^2 \right\rangle = \frac{\eta}{2} v^2 \text{Re} \left[\Pi_\omega^2(\mathbf{r}_1, \mathbf{r}_2) - \frac{1}{\mathcal{A}^2} \int d\mathbf{r}_2 d\mathbf{r}_2 \Pi_\omega^2(\mathbf{r}_1, \mathbf{r}_2) \right] \quad (\text{A3})$$

and $R_2 \approx 1$. We again have discarded the short-range terms proportional to k_d , assuming that the distance between the tips is much longer than the wavelength. Here

$$\Pi_\omega(\mathbf{r}_1, \mathbf{r}_2) = \frac{1}{\pi v} \sum_q \frac{\phi_q(\mathbf{r}_1) \phi_q(\mathbf{r}_2)}{\hbar D q^2 - i\omega}, \quad (\text{A4})$$

where Dq^2 and ϕ_q are the eigenfunctions and the eigenvalues of the diffusion operator $-D\nabla^2$ with appropriate boundary conditions. Note that at $\omega = 0$, $\Pi_{\omega=0}(\mathbf{r}_1, \mathbf{r}_2) = \Pi(\mathbf{r}_1, \mathbf{r}_2)$.

To facilitate the calculations, we take $V_1 = V_2 = V$. Since $R(\omega)$ and Π_ω are even functions of ω , we can reduce the double integral to a single one using

$$\int_0^{eV} dE_1 dE_2 F(E_1 - E_2) = 2 \int_0^{eV} (eV - \omega) F(\omega) d\omega, \quad (\text{A5})$$

where F is an arbitrary even function of ω . Due to nontrivial dependences of our functions on ω , we consider different regimes in voltage.

1. Regime 1: $eV \ll \Delta$

For $eV \ll \Delta$ in GUE we substitute Eq. (A1) for $R(\omega)$ and calculate

$$\int_0^{eV} (eV - \omega)R(\omega)d\omega \approx \frac{\pi^2}{36\Delta^2}(eV)^4, \quad (\text{A6})$$

and the contribution to the current correlations from the last term in Eq. (5) becomes

$$\delta J(\mathbf{r}_1, \mathbf{r}_2; V, V) = \frac{\pi^2 v^2 B_1 B_2}{36\Delta^2} (eV)^4 \Pi^2(\mathbf{r}_1, \mathbf{r}_2). \quad (\text{A7})$$

This differs from Eq. (10) by a factor of $g^{-1}(eV/\Delta)^3 \ll 1$.

For GOE, the level correlation function is cumbersome, but we need only the low-energy behavior, which is $R(\omega) \approx (\pi^2|\omega|)/(6\Delta)$. Calculating the current correlation function, we obtain

$$\delta J(\mathbf{r}_1, \mathbf{r}_2; V, V) = \frac{\pi^2 v^2 B_1 B_2}{36\Delta} (eV)^3 \Pi^2(\mathbf{r}_1, \mathbf{r}_2). \quad (\text{A8})$$

It is the same as Eq. (A7), except for the additional factor $\Delta/eV \gg 1$, making it bigger than Eq. (A7). It is still a factor $g^{-1}(eV/\Delta)^2 \ll 1$ lower than the contribution of correlations of the same wave function.

2. Regime 2: $\Delta \ll eV \ll E_c$

For $\Delta \ll eV \ll E_c$ we have $R \approx 1$, and calculating the integral again, we find in both GOE and GUE

$$\delta J(\mathbf{r}_1, \mathbf{r}_2; V, V) = \frac{\pi^2 v^2 B_1 B_2 \eta}{2} (eV)^2 \Pi^2(\mathbf{r}_1, \mathbf{r}_2), \quad (\text{A9})$$

which is again small compared with Eq. (10) as $eV/E_c \ll 1$.

3. Regime 3: $E_c \ll eV \ll \hbar D/r^2$

For $eV \gg E_c$, we still have $R = 1$ but now need to use Eq. (A3) to calculate the current-current correlation. To get

the results, we now explicitly calculate Π_ω in two dimensions. In (A4), we take $\phi_q(\mathbf{r}) = \mathcal{A}^{-1/2} \exp(i\mathbf{q}\mathbf{r})$ and replace the summation over q with integration. Integrating over the angle, we get the Bessel functions, and subsequently, integrating over the length of q , we obtain Kelvin functions kei and ker ,

$$\begin{aligned} \text{Re } \Pi_\omega(\mathbf{r}_1, \mathbf{r}_2) \\ = \frac{1}{4\pi^6 v^2 \hbar^2 D^2} \left[\text{kei}^2 \left(\sqrt{\frac{\omega}{\hbar D}} r \right) + \text{ker}^2 \left(\sqrt{\frac{\omega}{\hbar D}} r \right) \right]. \end{aligned} \quad (\text{A10})$$

In the case of $E_c \ll eV \ll \hbar D/r^2$, we can use the expansion of the Kelvin functions at low arguments, $\text{kei}, \text{ker}(x) = C, C' - (x/2)^2 \ln(x/2)$, where C and C' are two constants of the order of 1. We get

$$\delta J(\mathbf{r}_1, \mathbf{r}_2; V, V) \sim \frac{(C + C')v^2 B_1 B_2 \sigma}{2\pi^4 g^2} \frac{(eV)^3}{\hbar D/r^2} \ln \frac{\hbar D/r^2}{eV}. \quad (\text{A11})$$

Comparing this with the first term in J , we get

$$\delta J/J \sim \frac{1}{\pi^4} \frac{(eV)^2}{E_c \hbar D/r^2} \ln \frac{\hbar D/r^2}{eV}, \quad (\text{A12})$$

which in principle can become big but in practice is unlikely due to the small factor π^{-4} in front of this ratio.

4. Regime 4: $E_c \gg \hbar D/r^2$

In this case, we can replace $(eV - \omega)$ with eV in the integral over ω , and the remaining integral can be calculated exactly. The result is exponentially small ($\exp[-(2eVr^2/\hbar D)^{1/2}]$) and does not play any role.

Note that this regime makes sense only for $r \gg l$; then $\hbar D/r^2 \ll 1/\tau$, where τ is the momentum relaxation time for scattering at impurities. If $eV \gg 1/\tau$, the electron motion at highest energies is not diffusive, and our approach is no longer valid.

-
- [1] Q. Niu, M. C. Chang, and C. K. Shih, *Phys. Rev. B* **51**, 5502 (1995).
- [2] J. M. Byers and M. E. Flatté, *Phys. Rev. Lett.* **74**, 306 (1995).
- [3] M. Settnes, S. R. Power, D. H. Petersen, and A.-P. Jauho, *Phys. Rev. Lett.* **112**, 096801 (2014).
- [4] M. Settnes, S. R. Power, D. H. Petersen, and A.-P. Jauho, *Phys. Rev. B* **90**, 035440 (2014).
- [5] S. Hasegawa, *Roadmap of Scanning Probe Microscopy* (Springer, Berlin, 2007), Chap. 12.
- [6] B. Voigtländer, V. Cherepanov, S. Korte, A. Leis, D. Cuma, S. Just, and F. Lüpke, *Rev. Sci. Instrum.* **89**, 101101 (2018).
- [7] M. Kolmer, P. Olszowski, R. Zuzak, S. Godlewski, C. Joachim, and M. Szymanski, *J. Phys. Condens. Matter* **29**, 444004 (2017).
- [8] O. Kubo, Y. Shingaya, M. Nakaya, M. Aono, and T. Nakayama, *Appl. Phys. Lett.* **88**, 254101 (2006).
- [9] H. Konishi, Y. Murata, W. Wongwiriyan, M. Kishida, K. Tomita, K. Motoyoshi, S. Honda, M. Katayama, S. Yoshimoto, K. Kubo *et al.*, *Rev. Sci. Instrum.* **78**, 013703 (2007).
- [10] S. Yoshimoto, Y. Murata, K. Kubo, K. Tomita, K. Motoyoshi, T. Kimura, H. Okino, R. Hobara, I. Matsuda, S.-i. Honda *et al.*, *Nano Lett.* **7**, 956 (2007).
- [11] I. Shiraki, F. Tanabe, R. Hobara, T. Nagao, and S. Hasegawa, *Surf. Sci.* **493**, 633 (2001).
- [12] T.-H. Kim, Z. Wang, J. F. Wendelken, H. H. Weitering, W. Li, and A.-P. Li, *Rev. Sci. Instrum.* **78**, 123701 (2007).
- [13] R. Hobara, N. Nagamura, S. Hasegawa, I. Matsuda, Y. Yamamoto, Y. Miyatake, and T. Nagamura, *Rev. Sci. Instrum.* **78**, 053705 (2007).
- [14] O. Guise, H. Marbach, J. T. Yates, Jr., M.-C. Jung, J. Levy, and J. Ahner, *Rev. Sci. Instrum.* **76**, 045107 (2005).
- [15] R. Ma, Q. Huan, L. Wu, J. Yan, Q. Zou, A. Wang, C. A. Bobisch, L. Bao, and H.-J. Gao, *Rev. Sci. Instrum.* **88**, 063704 (2017).
- [16] H. Okamoto and D. Chen, *Rev. Sci. Instrum.* **72**, 4398 (2001).
- [17] R. Thamankar, T. Yap, K. Goh, C. Troadec, and C. Joachim, *Appl. Phys. Lett.* **103**, 083106 (2013).

- [18] M. Kolmer, P. Brandimarte, J. Lis, R. Zuzak, S. Godlewski, H. Kawai, A. Garcia-Lekue, N. Lorente, T. Frederiksen, C. Joachim *et al.*, *Nat. Commun.* **10**, 1573 (2019).
- [19] T. Siahhaan, O. Kurnosikov, B. Barcones, H. Swagten, and B. Koopmans, *Nanotechnology* **27**, 03LT01 (2015).
- [20] H. T. Ciftci, L. P. Van, B. Koopmans, and O. Kurnosikov, *J. Phys. Chem. A* **123**, 8036 (2019).
- [21] M. Leeuwenhoek, R. A. Norte, K. M. Bastiaans, D. Cho, I. Battisti, Y. M. Blanter, S. Gröblacher, and M. P. Allan, *Nanotechnology* **30**, 335702 (2019).
- [22] Y. S. Chan, Ph.D. thesis, Harvard University, 1997.
- [23] S. Tsukamoto, B. Siu, and N. Nakagiri, *Rev. Sci. Instrum.* **62**, 1767 (1991).
- [24] P. Jaschinsky, P. Coenen, G. Pirug, and B. Voigtländer, *Rev. Sci. Instrum.* **77**, 093701 (2006).
- [25] J. Yang, D. Sordes, M. Kolmer, D. Martrou, and C. Joachim, *Eur. Phys. J. Appl. Phys.* **73**, 10702 (2016).
- [26] V. Cherepanov, E. Zubkov, H. Junker, S. Korte, M. Blab, P. Coenen, and B. Voigtländer, in *Atomic Scale Interconnection Machines* (Springer, Heidelberg, 2012), pp. 9–21.
- [27] L. Gurevich, L. Canali, and L. P. Kouwenhoven, *Appl. Phys. Lett.* **76**, 384 (2000).
- [28] P. Boggild, T. M. Hansen, O. Kuhn, F. Grey, T. Junno, and L. Montelius, *Rev. Sci. Instrum.* **71**, 2781 (2000).
- [29] M. Nagase, H. Hibino, H. Kageshima, and H. Yamaguchi, *Nanotechnology* **19**, 495701 (2008).
- [30] N. Khotkevych, Y. Kolesnichenko, and J. van Ruitenbeek, *Low Temp. Phys.* **37**, 53 (2011).
- [31] T. Gramspacher and M. Büttiker, *Phys. Rev. Lett.* **81**, 2763 (1998).
- [32] T. Gramspacher and M. Büttiker, *Phys. Rev. B* **60**, 2375 (1999).
- [33] Ya. M. Blanter and A. D. Mirlin, *Phys. Rev. E* **55**, 6514 (1997).
- [34] A. D. Mirlin, *Phys. Rep.* **326**, 259 (2000).
- [35] C. J. Chen, *Introduction to Scanning Tunneling Microscopy* (Oxford University Press, Oxford, 1993).
- [36] S. Lounis, [arXiv:1404.0961](https://arxiv.org/abs/1404.0961).
- [37] Ya. M. Blanter, A. D. Mirlin, and B. A. Muzykantskii, *Phys. Rev. B* **63**, 235315 (2001).
- [38] L. Liu, W. Xiao, K. Yang, L. Zhang, Y. Jiang, X. Fei, S. Du, and H.-J. Gao, *J. Phys. Chem. C* **117**, 22652 (2013).
- [39] S. Bose, A. M. García-García, M. M. Ugeda, J. D. Urbina, C. H. Michaelis, I. Brihuega, and K. Kern, *Nat. Mater.* **9**, 550 (2010).
- [40] J. Kim, G. A. Fiete, H. Nam, A. H. MacDonald, and C.-K. Shih, *Phys. Rev. B* **84**, 014517 (2011).
- [41] S. Rolf-Pissarczyk, J. A. J. Burgess, S. Yan, and S. Loth, *Phys. Rev. B* **94**, 224504 (2016).
- [42] R. Eichele, W. Kern, and R. P. Huebener, *Appl. Phys.* **25**, 95 (1981).
- [43] N. Ashcroft and N. Mermin, *Solid State Physics* (Saunders College, Philadelphia, 1976), p. 38.